

Control of ferroelectric polarization via uniaxial pressure in the spin-lattice-coupled multiferroic $\text{CuFe}_{1-x}\text{Ga}_x\text{O}_2$

T. Nakajima,^{1,*} S. Mitsuda,¹ T. Nakamura,¹ H. Ishii,¹ T. Haku,¹ Y. Honma,¹ M. Kosaka,² N. Aso,³ and Y. Uwatoko⁴

¹*Department of Physics, Faculty of Science, Tokyo University of Science, Tokyo 162-8601, Japan*

²*Graduate School of Science and Engineering, Saitama University, Saitama, Saitama 338-8570, Japan*

³*Faculty of Science, University of the Ryukyus, Nishihara, Okinawa 903-0213, Japan*

⁴*Institute for Solid State Physics, University of Tokyo, Kashiwa, Chiba 277-8581, Japan*

We have demonstrated that ferroelectric polarization in a spin-driven multiferroic $\text{CuFe}_{1-x}\text{Ga}_x\text{O}_2$ with $x = 0.035$ can be controlled by the application of uniaxial pressure. Our neutron diffraction and in-situ ferroelectric polarization measurements have revealed that the pressure dependence of the ferroelectric polarization is explained by repopulation of three types of magnetic domains originating from the trigonal symmetry of the crystal. We conclude that the spin-driven anisotropic lattice distortion and the fixed relationship between the directions of the magnetic modulation wave vector and the ferroelectric polarization are the keys to this spin-mediated piezoelectric effect.

PACS numbers: 75.85.+t, 75.25.-j

Magnetic frustration induces a variety of cross-correlated phenomena in condensed matter. For example, frustrated magnets often exhibit anisotropic lattice distortion associated with magnetic order, in order to lift the degeneracy due to competing magnetic interactions^{1,2}. In other words, spin and lattice degrees of freedom are tightly coupled with each other in frustrated magnets. Another example is spin-driven ferroelectricity. Frustrated magnets often display complex noncollinear magnetic orderings, some of which break the inversion symmetry of a system. Recent studies on magneto-electric (ME) multiferroics have revealed that magnetic inversion symmetry breaking accounts for the ferroelectricity³⁻⁵. Based on the relationships among the spin, lattice and dielectric degrees of freedom in frustrated magnets, we have demonstrated that spin-driven ferroelectric polarization is controlled by pressure, which directly affects the lattice degree of freedom, in the spin-lattice-coupled ME multiferroic $\text{CuFe}_{1-x}\text{Ga}_x\text{O}_2$ (CFO) with $x = 0.035$.

The delafossite compound CuFeO_2 (CFO) is a triangular lattice antiferromagnet, which is a typical example of frustrated spin system. Because of antiferromagnetic interactions between the magnetic Fe^{3+} ions forming the triangular lattice, this system has strong magnetic frustration and it therefore exhibits a variety of unconventional magnetic phase transitions^{6,7}. Despite the Heisenberg spin character expected from the electronic state of the magnetic Fe^{3+} ions ($S = \frac{5}{2}, L = 0$), CFO exhibits an Ising-like collinear four-sublattice (4SL) magnetic ground state. A small amount of nonmagnetic substitution or the application of a magnetic field turns the 4SL phase to a noncollinear incommensurate magnetic phase, in which spin-driven ferroelectricity has been discovered⁸⁻¹⁰. Hereafter, we refer to this ferroelectric phase as the ‘ferroelectric incommensurate magnetic (FE-ICM) phase’. The magnetic structure of the FE-ICM phase has been determined to be an elliptical screw-type magnetic structure, whose magnetic modu-

lation wave vector is $(q, q, \frac{3}{2})$ with $q = 0.203$ ^{11,12}. Spin-driven ferroelectric polarization emerges along the screw axis, which is parallel to the [110] direction of the crystal. The polarity of the ferroelectric polarization is coupled with the chirality of the magnetic structure, i.e., the left-handed (LH) and right-handed (RH) helical arrangements of the spins^{12,13}.

CFO also exhibits spin-driven crystal structural transitions. Recent synchrotron radiation x-ray diffraction studies have revealed that CFO exhibits monoclinic lattice distortions in several magnetically ordered phases including the FE-ICM phase¹⁴⁻¹⁷, while CFO has a trigonal crystal structure in the paramagnetic (PM) phase. This spin-driven structural transition produces three types of monoclinic crystal domains because the original trigonal crystal structure has a threefold rotational symmetry about the c axis. The relationships between the hexagonal and the monoclinic bases in each domain are shown in Figs. 1(a)-1(c). Note that in this letter, we have mainly employed the hexagonal basis to describe the three types of domains. We have added subscripts ‘m’ when referring to the monoclinic bases. In each monoclinic domain, the b_m axis elongates and, in contrast, the a_m axis contracts, compared to those in the PM phase. In addition, the c^* -plane-projection of the magnetic modulation wave vector, which is parallel to the screw axis in the FE-ICM phase, is fixed to be parallel to the b_m axis. Hereafter, we refer to the three types of coupled magnetic and crystal domains as (110)-, (1 $\bar{2}$ 0)- and ($\bar{2}$ 10)-domains, as shown in Figs. 1(a)-1(c). Taking account of the strong spin-lattice coupling in this system, we have recently demonstrated that in CFO, the volume fractions of the three magnetic domains can be controlled by uniaxial pressure applied perpendicular to the c axis¹⁸. We thus expect that in the FE-ICM phase, application of uniaxial pressure results in distinct changes in the ferroelectric polarization reflecting the changes in the volume fractions of the three magnetic domains. In the present study, we have performed neutron diffraction and in-situ ferroelectric polarization

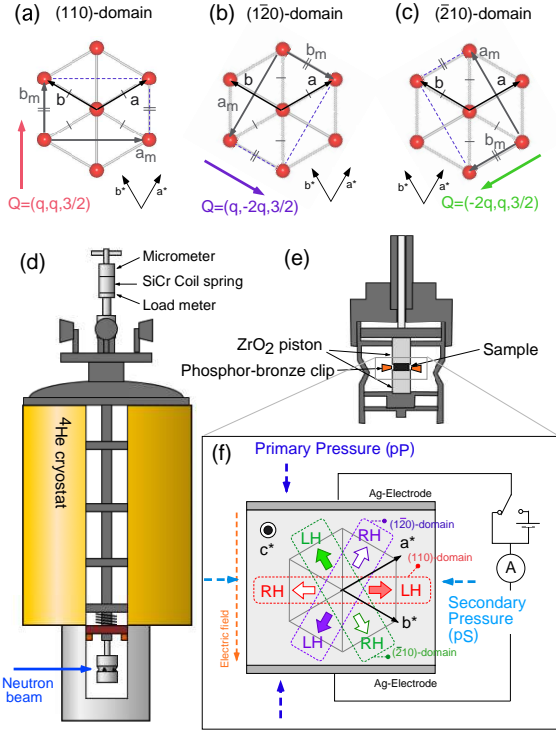


FIG. 1: (Color Online) [(a)-(c)] Relationships between the hexagonal and the monoclinic bases in the three types of domains. (d) Schematic drawing of the uniaxial pressure cell inserted in the cryostat. (e) Magnification of the sample space of the pressure cell. (f) Relationships among the six possible directions of the ferroelectric polarization, applied electric field and two directions of uniaxial pressure. Open and filled arrows denote the directions of the ferroelectric polarization induced by the RH- and the LH-helical magnetic domains, respectively.

measurements under applied uniaxial pressure, using a CFGO ($x = 0.035$) sample, which exhibits the FE-ICM phase below ~ 8 K in zero magnetic field.

A single crystal of CFGO ($x = 0.035$) of nominal composition was prepared by the floating zone method¹⁹ and was cut to dimensions of $\sim 2.9 \times 2.1 \times 4.0$ mm³ with the $[1\bar{1}0]$ direction parallel to the shortest dimension. We have developed a uniaxial pressure cell loaded into a pumped ^4He cryostat, as illustrated in Fig. 1(d). The uniaxial pressure along the vertical direction is controlled by a SiCr coil spring and a micrometer attached on top of the cryostat and is monitored by a load meter. The sample was mounted in the pressure cell with the (H, H, L) scattering plane orientated so that the vertical uniaxial pressure was applied to the $[1\bar{1}0]$ surfaces of the sample. Uniaxial pressure was also applied to the $[110]$ surfaces by a small phosphor-bronze clip. Hereafter, we refer to the vertical pressure applied by the spring and the horizontal pressure applied by the clip as ‘primary pressure’ (p_P) and ‘secondary pressure’ (p_S), respectively. In this experimental setup, we can control the magnitude of p_P

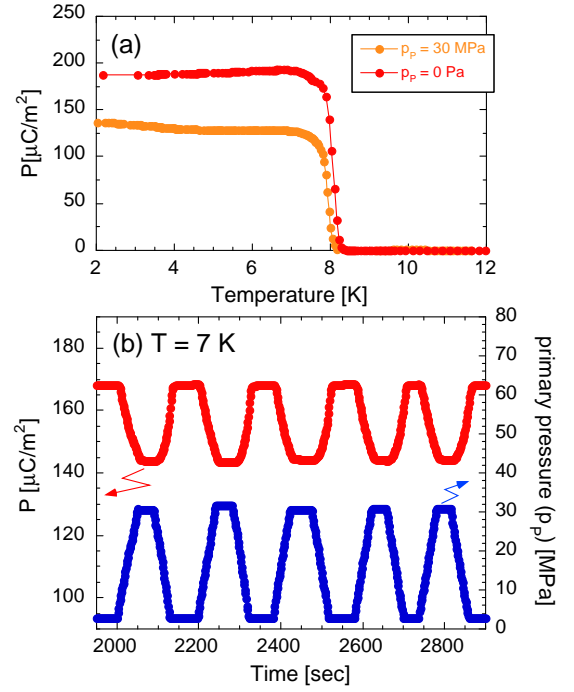


FIG. 2: (Color Online) (a) Temperature variations of P measured on heating at $p_P = 0$ and 30 MPa. (b) Time dependences of P and p_P at 7 K.

even at low temperatures. On the other hand, we cannot control p_S , which was kept applied throughout the present experiment. The magnitude of p_S is assumed to be relatively small. Silver paste electrodes were applied to the $[1\bar{1}0]$ surfaces of the sample. The ferroelectric polarization along the $[1\bar{1}0]$ direction (P) was deduced by integrating the pyroelectric or piezoelectric current measured by an electrometer. Neutron diffraction measurements under an applied uniaxial pressure were carried out with a triple axis spectrometer HQR installed in JRR-3 of the Japan Atomic Energy Agency in Tokai, Japan. The wavelength of the incident neutron beam was 2.44 Å, and the collimation was open-40°-40°-40°.

Figure 2(a) shows the temperature variations of P measured on heating at $p_P = 0$ and 30 MPa. We have found that the application of only 30 MPa of p_P significantly reduces the value of P . At 7 K, just below the ferroelectric transition temperature, we have measured the p_P -dependence of P in zero electric field²⁰. Before this measurement, the sample was cooled with an applied electric field of 116 kV/m from 10 K to 2 K, and then was heated to 7 K in zero electric field. In Fig. 2(b), we show the values of P and p_P as functions of time²¹, revealing that the time dependence of P is synchronized with that of p_P : P gradually decreases and increases with increasing and decreasing p_P , respectively.

Subsequent to the ferroelectric polarization measurement, we have performed neutron diffraction measurements. We have measured three magnetic Bragg re-

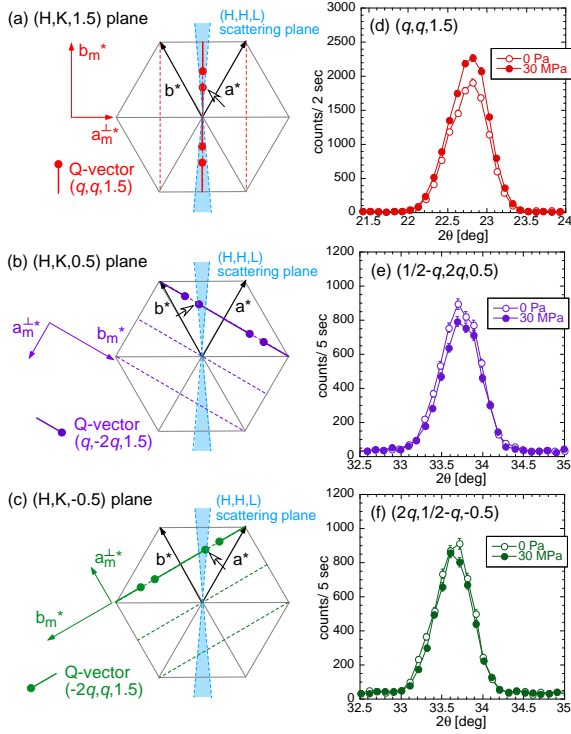


FIG. 3: (Color Online) [(a)-(c)] The locations of the magnetic Bragg reflections belonging to the (a) (110)-, (b) $(\bar{1}20)$ - and (c) $(\bar{2}10)$ -domains, in the reciprocal lattice space. a_m^\perp denotes the c^* -plane-projection of a_m^* . Open arrows denote the positions of the magnetic reflections corresponding to (d)-(f). Although the magnetic reflections belonging to the $(\bar{1}20)$ - and $(\bar{2}10)$ -domains do not appear on the (H,H,L) plane in principle, we can access the two reflections belonging to these domains by tilting the cryostat by $\pm \sim 4^\circ$. [(d)-(f)] Comparisons between the magnetic diffraction profiles measured at $p_P = 0$ and 30 MPa at 7 K

reflections at $(q, q, \frac{3}{2})$, $(\frac{1}{2} - q, 2q, \frac{1}{2})$ and $(2q, \frac{1}{2} - q, -\frac{1}{2})$, which belong to the (110)-, $(\bar{1}20)$ - and $(\bar{2}10)$ -domains, respectively. In Figs. 3(d)-3(f), we show the comparisons between the magnetic diffraction profiles measured at $p_P = 0$ and 30 MPa. We have found that the intensity of the $(q, q, \frac{3}{2})$ reflection is enhanced by the application of p_P . In contrast, those of the $(\frac{1}{2} - q, 2q, \frac{1}{2})$ and $(2q, \frac{1}{2} - q, -\frac{1}{2})$ reflections are reduced. This suggests that the volume fraction of the (110)-domain increases and those of the $(\bar{1}20)$ - and $(\bar{2}10)$ -domains decrease with increasing p_P . Since the ferroelectric polarization vector in the (110)-domain is parallel to the electrodes, the observed value of P is proportional to the sum of the volume fractions of the $(\bar{1}20)$ - and $(\bar{2}10)$ -domains. Therefore, the p_P dependences of the intensities of the magnetic Bragg reflections are consistent with the results of the ferroelectric polarization measurements.

Hereafter, we refer to the volume fractions of the (110)-, $(\bar{1}20)$ - and $(\bar{2}10)$ -domains as $V_{(110)}$, $V_{(\bar{1}20)}$ and $V_{(\bar{2}10)}$, respectively. The sum of the volume fractions relevant to

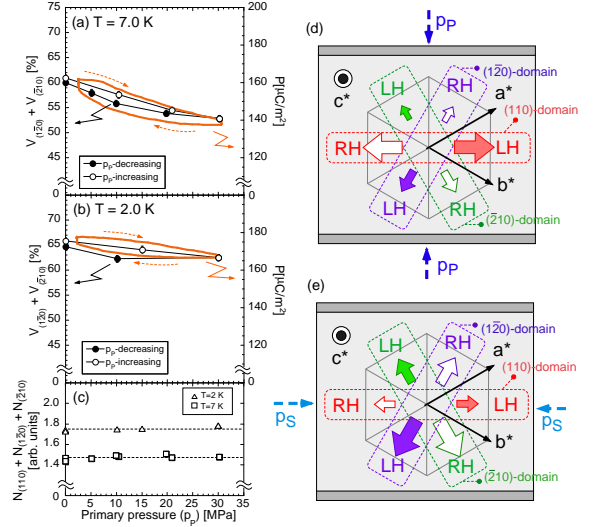


FIG. 4: (Color Online) [(a),(b)] Comparison between the p_P dependences of P and $V_{(\bar{1}20)} + V_{(\bar{2}10)}$ at (a) 7 K and (b) 2 K. The ratio of the scales of the vertical axes (P and $V_{(\bar{1}20)} + V_{(\bar{2}10)}$) is the same in (a) and (b). (c) p_P dependences of $N_{(110)} + N_{(\bar{1}20)} + N_{(\bar{2}10)}$ at 2 K and 7 K. [(d),(e)] Schematic drawings of the volume fractions of the coupled magnetic and ferroelectric domains (d) when the effect of p_P is dominant and (e) when the effect of p_S is dominant. Sizes of the open and filled arrows qualitatively show the volume fractions of the RH- and the LH-helical magnetic domains, respectively.

P is described by

$$P \propto V_{(\bar{1}20)} + V_{(\bar{2}10)} = \frac{N_{(\bar{1}20)} + N_{(\bar{2}10)}}{N_{(110)} + N_{(\bar{1}20)} + N_{(\bar{2}10)}}, \quad (1)$$

where N_α [$\alpha = (110), (\bar{1}20)$ or $(\bar{2}10)$] is the integrated intensity of the magnetic Bragg reflection belonging to the α -domain divided by the Lorentz factor and the square of the calculated magnetic structure factor for the magnetic reflection. It should be noted that the sum of $N_{(110)}$, $N_{(\bar{1}20)}$ and $N_{(\bar{2}10)}$ is independent of p_P , as shown in Fig. 4(c). This suggests that the application of 30 MPa of p_P does not affect the magnetic structure in the FE-ICM phase, and therefore the changes in the intensities of the magnetic Bragg reflections can be ascribed only to the changes in the volume fractions of the three domains. Figures 4(a) and 4(b) show the values of P and $V_{(\bar{1}20)} + V_{(\bar{2}10)}$ at 7 K and 2 K as functions of p_P .²² We have found that the p_P -variations of P agree with those of $V_{(\bar{1}20)} + V_{(\bar{2}10)}$ at both temperatures. This indicates that the changes in P are explained by the pressure-induced repopulation of the three magnetic domains. Specifically, the uniaxial pressure along the $[1\bar{1}0]$ direction favors the domains whose a_m axis lies along the direction of the pressure, and suppresses the other domains, because of the anisotropic lattice distortion in each domain. Hence, $V_{(\bar{1}20)}$ and $V_{(\bar{2}10)}$ decrease with increasing p_P , as illustrated in Fig. 4(d). When p_P is removed and the effect of p_S is dominant, p_S suppresses the magnetic domains

whose b_m axis are parallel to p_S and enhances the other domains, and therefore $V_{(1\bar{2}0)}$ and $V_{(\bar{2}10)}$ increase with decreasing p_P , as illustrated in Fig. 4(e). It should be noted that $V_{(1\bar{2}0)}$ and $V_{(\bar{2}10)}$ might not be retrieved without the application of p_S .

We now discuss the microscopic picture of the domain structures in this system. The fact that the p_P -variations of P are proportional to those of $V_{(1\bar{2}0)} + V_{(\bar{2}10)}$ indicates that the asymmetry of the LH- and the RH-helical magnetic orderings in each of the (110), $(1\bar{2}0)$ or $(\bar{2}10)$ -domains remain unchanged even after the volume fractions of the three domains change. This implies that the domain walls separating the three types of crystal domains gradually move with increasing or decreasing pressure, keeping the asymmetry of the LH- and the RH-helical magnetic orderings in each of the domains. In other words, sudden flops or reconstruction of the crystal domains, in which the magnetic chirality might be no longer conserved, hardly occur in the present experiments. The present results also suggest that mobility of the domain walls are reduced at low temperatures.

In conclusion, we have demonstrated uniaxial pressure control of ferroelectric polarization in a frustrated magnet $\text{CuFe}_{1-x}\text{Ga}_x\text{O}_2$ with $x = 0.035$, in which the spin,

lattice and dielectric degrees of freedom are tightly coupled with each other. The present neutron diffraction and in-situ ferroelectric polarization measurements have revealed that the application of uniaxial pressure along the $[1\bar{1}0]$ direction results in repopulation of the three types of coupled crystal and magnetic domains owing to the spin-driven anisotropic lattice distortions in each domain. Consequently, the ferroelectric polarization along the $[1\bar{1}0]$ direction changes with the applied pressure, reflecting the domain structure in the sample. Although the present work has focused only on the pressure dependence of the domain structure, we expect that spin-frustrated magnets have the potential to show a variety of pressure-induced cross correlated phenomena including this kind of spin-mediated piezoelectric effect.

ACKNOWLEDGMENTS

The neutron diffraction measurements at JRR-3 were carried out as part of proposal 10695B and were partly supported by ISSP of the University of Tokyo.

-
- * Electronic address: E-mail address: nakajima@nsmsmac4.ph.kagun.tokai.ac.jp
- ¹ Y. Yamashita and K. Ueda, Phys. Rev. Lett. **85**, 4960 (2000).
 - ² K. Penc, N. Shannon, and H. Shiba, Phys. Rev. Lett. **93**, 197203 (2004).
 - ³ T. Kimura, T. Goto, H. Shintani, K. Ishizaka, T. Arima, and Y. Tokura, Nature (London) **426**, 55 (2003).
 - ⁴ H. Katsura, N. Nagaosa, and A. V. Balatsky, Phys. Rev. Lett. **95**, 057205 (2005).
 - ⁵ M. Kenzelmann, A. B. Harris, S. Jonas, C. Broholm, J. Schefer, S. B. Kim, C. L. Zhang, S.-W. Cheong, O. P. Vajk, and J. W. Lynn, Phys. Rev. Lett. **95**, 087206 (2005).
 - ⁶ S. Mitsuda, H. Yoshizawa, N. Yaguchi, and M. Mekata, J. Phys. Soc. Jpn. **60**, 1885 (1991).
 - ⁷ S. Mitsuda, M. Mase, K. Prokes, H. Kitazawa, and H. A. Katori, J. Phys. Soc. Jpn. **69**, 3513 (2000).
 - ⁸ T. Kimura, J. C. Lashley, and A. P. Ramirez, Phys. Rev. B **73**, 220401(R) (2006).
 - ⁹ S. Seki, Y. Yamasaki, Y. Shiomi, S. Iguchi, Y. Onose, and Y. Tokura, Phys. Rev. B **75**, 100403(R) (2007).
 - ¹⁰ N. Terada, T. Nakajima, S. Mitsuda, H. Kitazawa, K. Kaneko, and N. Metoki, Phys. Rev. B **78**, 014101 (2008).
 - ¹¹ T. Nakajima, S. Mitsuda, S. Kanetsuki, K. Prokes, A. Podlesnyak, H. Kimura, and Y. Noda, J. Phys. Soc. Jpn. **76**, 043709 (2007).
 - ¹² T. Nakajima, S. Mitsuda, K. Takahashi, M. Yamano, K. Masuda, H. Yamazaki, K. Prokes, K. Kiefer, S. Gerischer, N. Terada, et al., Phys. Rev. B **79**, 214423 (2009).
 - ¹³ T. Nakajima, S. Mitsuda, S. Kanetsuki, K. Tanaka, K. Fujii, N. Terada, M. Soda, M. Matsuura, and K. Hirota, Phys. Rev. B **77**, 052401 (2008).
 - ¹⁴ T. Nakajima, S. Mitsuda, H. Ohsumi, and K. Tajima, J. Phys. Soc. Jpn. **75**, 023602 (2006).
 - ¹⁵ F. Ye, Y. Ren, Q. Huang, J. A. Fernandez-Baca, P. Dai, J. W. Lynn, and T. Kimura, Phys. Rev. B **73**, 220404(R) (2006).
 - ¹⁶ N. Terada, Y. Tanaka, Y. Tabata, K. Katsumata, A. Kikkawa, and S. Mitsuda, J. Phys. Soc. Jpn. **75**, 113702 (2006).
 - ¹⁷ T. Nakajima, S. Mitsuda, T. Inami, N. Terada, H. Ohsumi, K. Prokes, and A. Podlesnyak, Phys. Rev. B **78**, 024106 (2008).
 - ¹⁸ T. Nakajima, S. Mitsuda, T. Haku, K. Shibata, K. Yoshitomi, Y. Noda, N. Aso, Y. Uwatoko, and N. Terada, J. Phys. Soc. Jpn. **80**, 014714 (2011).
 - ¹⁹ T. R. Zhao, M. Hasegawa, and H. Takei, J. Cryst. Growth **166**, 408 (1996).
 - ²⁰ After the piezoelectric and the neutron diffraction measurements shown in Figs. 2(b), 4(a) and 4(b), we have performed pyroelectric measurements with increasing temperature beyond T_c to determine the absolute values of P in Figs. 2(b), 4(a) and 4(b).
 - ²¹ The measurements of Figs. 2(b) and 3 were performed after several pressure cycles at 7 K. After the first pressure cycle, the maximum value of the ferroelectric polarization (at zero pressure) decreased from $\sim 185 \mu\text{C}/\text{m}^2$ to $\sim 170 \mu\text{C}/\text{m}^2$, but it didn't change in the 2nd cycle and later.
 - ²² The p_P -variations of the volume fractions shown in Figs. 4(a) and 4(b) are rather small as compared to those in the previous study¹⁸. This is because the effect of the secondary pressure (not applied in the previous work) conflicts with that of the primary pressure. As a result, the sensitivity to p_P is reduced.